Assessment of different methods of analysis to characterise the mixing of shear-thinning fluids in a Kenics KM static mixer using PLIF

CrossMark

F. Alberini [a], M.J.H. Simmons [a,*], A. Ingram [a], E.H. Stitt [b]

[a] School of Chemical Engineering, University of Birmingham, B15 2 TT, UK
[b] Johnson Matthey Technology Centre, Billingham TS23 1LB, UK

HIGHLIGHTS

- Analysis of PLIF images of KM static mixers using non-Newtonian aqueous solutions.
- Analysis of the data using CoV and striation area gives misleading results.
- Analysis of striation area distribution is presented.
- Effect of scale, velocity, flow ratio and different injection are detected.
- Wall injection negatively affects the overall mixing performance.

ABSTRACT

The performance of Kenics KM static mixers has been determined for the blending of two shear-thinning fluid streams with identical or different rheology. Planar Laser Induced Fluorescence (PLIF) has been used to obtain the concentration distribution at the mixer outlet by doping one fluid stream with fluorescent dye upstream of the mixer inlet. The effect of scale of the static mixer, total flow rate, flow ratio between the fluid streams and inlet configuration have been investigated. The applicability of different methods to characterise mixing performance is examined by comparing conventional mixing measures such as coefficient of variation and maximum striation area against recent alternative methods presented in the literature, such as the areal distribution method developed by Alberini et al. (2014). A method of characterising individual striations by determining their distribution as a function of size and concentration is also presented. These findings illustrate the complexity of information-rich PLIF images, and highlight how different methods of analysis may be appropriate given the dependencies of the downstream process.

© 2014 The Authors. Published by Elsevier Ltd. This is an open access article under the CC BY license (http://creativecommons.org/licenses/by/3.0/).

1. Introduction

For industries manufacturing complex fluid products to remain competitive in the global marketplace, maintenance and retention of leading edge technical capabilities for the development of new products and their manufacture are both vital. Across many sectors including food, pharmaceuticals and catalysis, these fluid products possess a complex (non-Newtonian) rheology which needs to be understood to ensure process operability. Whilst most processing of complex fluids has been carried out traditionally in batch plant, continuous processing is becoming increasingly attractive due to lower energy costs, decreased plant footprint and reduced inventory. However, development of reliable continuous plant requires

that the capabilities of each unit operation are well understood; in terms of mixing and blending operations the in-line static mixer is a common choice and has established itself as a workhorse of the chemical industry (Etchells and Meyer, 2004).

Whilst there is a reasonable amount of data and design information available for the blending of Newtonian materials using static mixers (e.g. Shah and Kale, 1991), and consequently analysis of mixing performance characterising the influence of viscosity (Ventresca et al., 2002), there is a comparative dearth of published material on non-Newtonian mixing. Understanding of the blending of non-Newtonian fluids has concentrated upon fluid dynamical aspects, which tend to focus on measured pressure drop as a function of rheology (Chandra and Kale, 1992), or on the determination of velocity profiles, (e.g. for the Kenics (KM) static mixer using Laser Doppler Anemometry (Adamiak and Jaworski, 2001; Peryt-Stawiarska and Jaworski, 2011)) or on generating 3D Eulerian velocity maps using Positron Emission Particle Tracking (PEPT)

(Rafiee et al., 2013) rather than mixing quality. Tozzi et al. (2012) used a different approach to determine mixing performance in static mixers by quantifying the mixedness from rheological perturbations using Magnetic Resonance Imaging (MRI).

Whilst these fundamental data are valuable for the verification of Computational Fluid Dynamics (CFD) simulations (e.g. Peryt-Stawiarska and Jaworski, 2008; Rahmani and Keith, 2006), they do not allow the mixing performance to be determined ab initio and there is an absence of experimental work (using non-Newtonian fluids) where an analysis based upon the concentration distribution in the pipe cross-section at the mixer outlet is performed. This is the most direct way to determine if two fluids are mixed. The choice of method or algorithm used to determine mixing performance is of critical importance. The traditional approach for the calculation of mixing quality in low Reynolds number (laminar) flows is to assess the distribution of the concentration of a passive scalar, C_i, via statistical methods. This leads to the calculation of parameters such as the *coefficient of variation* (CoV) as described in Etchells and Meyer (2004) or striation thickness (Kukukova et al., 2011). CoV is the ratio of the standard deviation of the concentration distribution in the mixing field (intensity of segregation), σ, divided by the concentration which would be expected for complete mixing, $\overline{C}$, shown in Eq. (1). Striation thicknesses or areas (scale of segregation) are usually obtained via image analysis of the concentration field.

$$\text{CoV} = \frac{\sigma}{\overline{C}} = \frac{1}{N}\sum_N \frac{\sqrt{(C_i - \overline{C})^2}}{\overline{C}} \qquad (1)$$

Different approaches to obtain the scale of segregation have been compared by Kukukova et al. (2011); they found that determination of the area of the largest striation, termed the *maximum striation area*, was the fastest method in terms of processing time, but that this analysis was limited in its description of the whole mixing field. They illustrated other approaches to characterise mixing which provided more information but led to higher processing times; a common factor is the assumption of improved mixing with a decrease in maximum striation area (Spencer and Wiley, 1951), but this does not consider the concentration, or degree of mixing within the striation.

The chaotic nature of the flow patterns within the static mixer lead to a mixing pattern whose complexity cannot be captured by one simple numerical measure based upon either a length (or area) scale or concentration variance. Indeed, considering either of these measures in isolation may lead to highly misleading conclusions to be drawn (Kukukova et al., 2009). A thorough analysis therefore requires these aspects to be considered together; this is the basis of the *areal distribution method* recently published by Alberini et al. (2014). In this method, concentration distributions in the pipe cross-section at the mixer outlet (obtained using PLIF) are analysed on a pixel by pixel basis and the level of mixedness, X, is calculated for each pixel. The parameter X is simply related to the CoV. A CoV of zero corresponds to perfect ($X = 100\%$) mixing, where $C_i = \overline{C}$ in the pixel. Similarly a pixel value of CoV of 0.1 is equivalent to $X = 90\%$. Then the pixels are binned according to their value of X which enables a distribution of the fraction of the total cross sectional area to be plotted as a function of X. Implementation and more details of the method may be found in Alberini et al. (2014) and in §3.2 in this paper. This method was developed in particular to analyse the effect of blending a minor (secondary) flow into a major primary flow. This laminar mixing duty becomes challenging when the secondary flow has a significantly higher apparent viscosity than the primary flow, leading to the formation of viscous filaments whose diffusion timescales are long compared with the process. Thus these filaments are very difficult to eliminate, yet this is a common industrial problem in the blending

of thickeners or slurries. Alberini et al. (2014) showed that the striations generated by the mixing of transparent model fluids, whose rheological properties were chosen to mimic industrial slurries, have a complicated lamellar structure with a strongly asymmetric distribution in the pipe cross-section.

This paper examines the effect of changing system and fluid parameters upon the mixing performance of a Kenics KM static mixer equipped with six elements for the blending of two shear thinning fluids, where a minor secondary flow is blended into a major primary flow. The physical parameters examined are total fluid superficial velocity (0.1–0.6 m s^{-1}), pipe internal diameter (0.0127–0.0254 m), the volumetric flow ratio between the primary and secondary flows (10:1 and 25:1) and changing the rheology of the secondary flow. Finally, the effect of the position of injection of the secondary flow at the mixer inlet, either at the centre or at the wall, is considered. The performance of the mixer is assessed by analysis of PLIF images using the traditional CoV and *maximum striation area* methods and the *areal distribution* method all outlined above. In addition, a fourth method, the *individual striation method,* is introduced which identifies the area and perimeter of individual striations within the cross section as a function of their level of mixedness, X. This method, described in §3.3 below, enables the size and mixedness of individual striations to be compared quantitatively as a function of changing process and fluid conditions.

2. Materials and methods

2.1. Static mixer experimental rig.

Fig. 1a is an overall schematic of the experimental rig and Fig. 1b is a detailed schematic of the static mixer test section. Kenics KM static mixer sections of pipe internal diameter, $D = 12.7$ mm (1/2″) and $D = 25.4$ mm (1″) are used, both equipped with 6 single blade 180 degree twisted elements (of $L/D = 1.5$) with lengths, $L = 0.11$ m and $L = 0.22$ m respectively. For the 1/2″ mixer, the primary flow is delivered by a Liquiflo gear pump controlled using a motor drive (Excal Meliamex Ltd.) and monitored using an electromagnetic flow metre (Krohne). Flow to the 1″ mixer is delivered by an Albany rotary gear pump controlled using an inverter control WEG (model CF208). For both mixer scales, the secondary flow is premixed with fluorescent dye (Rhodamine 6G) to a fixed concentration and then introduced using a Cole-Parmer Micropump (GB-P35). The injection of doped fluid is in either the centre of the pipe or next to the pipe wall and very close to the initial mixer element as shown in Fig. 1c; this set up is slightly different from the previous work (Alberini et al., 2014) where the position of the inlet was placed at a distance of one pipe diameter from the first static mixer element.

To enable flow measurements to be made using PLIF, which requires optically transparent materials, a Tee piece is placed at the end of the mixer section which has a glass window inserted on the corner of the Tee, normal to the axis of the main pipe. A glass pipe section upstream of the Tee at the mixer section outlet, enclosed in a square glass sight box to minimise distortion, provides optical access for the laser sheet to illuminate the transverse section.

Two pressure transmitters were located both upstream (PR-35X/10 bar, Keller UK) and downstream (PR-35X/1 bar, Keller UK) of the static mixer section, enabling measurement of the pressure drop at a sampling rate of 5 Hz. The transducers were placed as close as possible to the mixer section, being mounted 4 pipe diameters before and after the section respectively (Fig. 1b). The pressure transmitters also incorporated PT100 thermocouples enabling fluid temperature to be monitored throughout the experiments. The temperature of the fluids was maintained at 22 °C to ensure fluid rheology remained constant. Pressure drop data was obtained for the
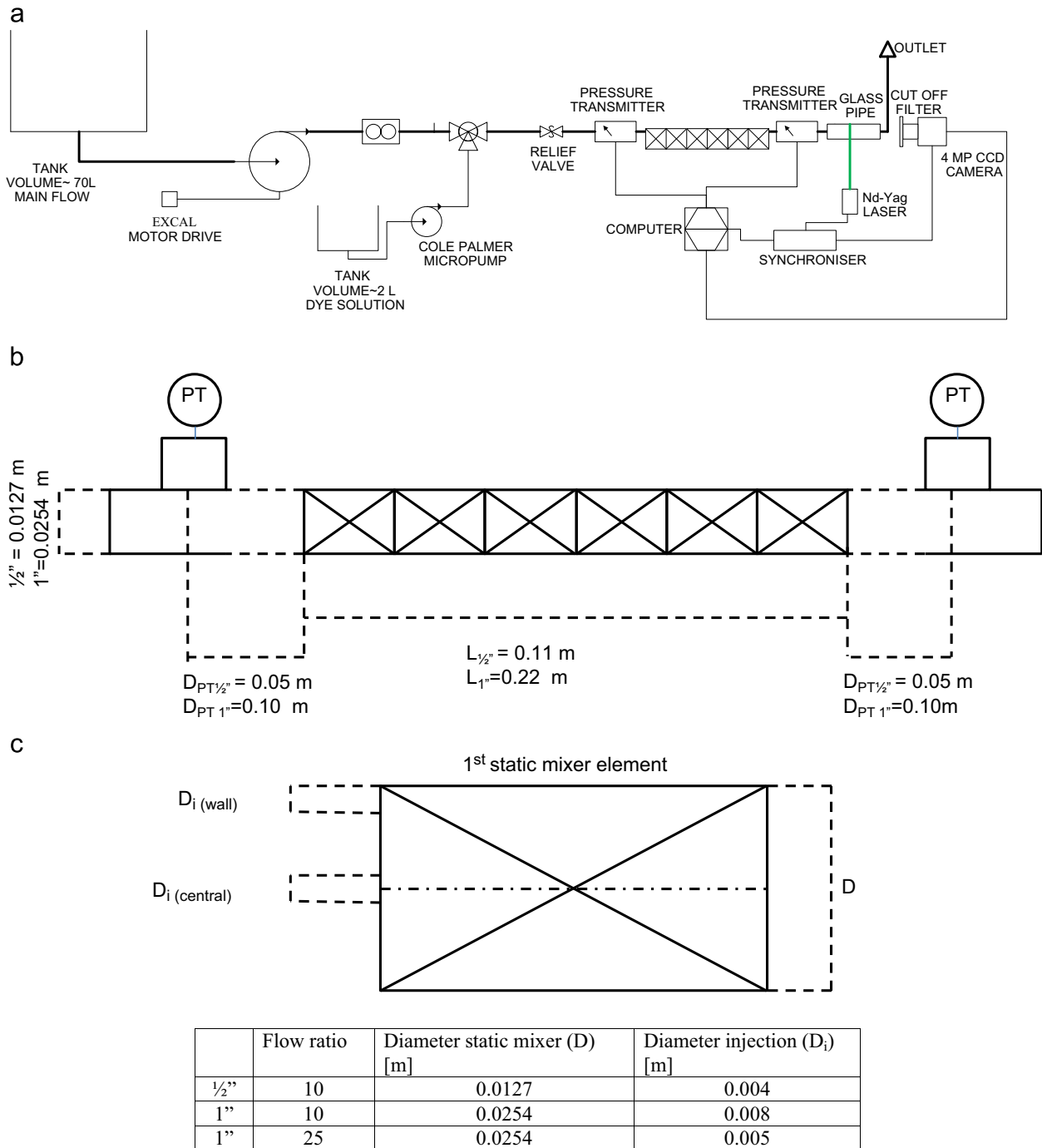
a

b

c

Fig. 1. Schematics of the static mixer test rig. (a) Overall schematic; (b) dimensions of static mixer test section showing location of pressure transducers; and (c) injection positions.

	Flow ratio	Diameter static mixer (D) [m]	Diameter injection (D$_i$) [m]
½"	10	0.0127	0.004
1"	10	0.0254	0.008
1"	25	0.0254	0.005

Table 1
Herschel–Bulkley model parameters obtained from rheological data for the aqueous Carbopol 940 solutions used in this study.

	Herschel Bulkley model $\tau = \tau_y + K\dot{\gamma}^n$		
	Yield stress τ_y (Pa)	Power law exponent n ($-$)	Consistency index K (Pa s^n)
Fluid 1: Solution 0.1% w/w pH=4.5	3.2	0.7	0.26
Fluid 2: Solution 0.2% w/w pH=5	25.2	0.42	6.74

continuous phase fluids over a range of superficial velocities, v, from $0.1 < v < 0.6$ m s^{-1} ($60 < Q < 300$ L h^{-1} for the 1/2" scale mixer and $180 < Q < 1080$ L h^{-1} for the 1" scale mixer). In Fig. 1c all the specifics of static mixer dimensions are reported including secondary flow inlet dimensions and injection position.

2.2. Fluids and flow conditions

The working fluids used were two different aqueous solutions of Carbopol 940 (Lubrizol Corp, Ohio, USA), a cross-linked polyacrylate polymer, which are miscible in each other. The rheology of both fluids was obtained using a cone and plate rheometer (TA AR1000, TA

Table 2
Experimental conditions.

Experiment	Injected fluid and position of injection	Superficial velocity v (m s^{-1})			Flow ratio (FR)	Pipe diameter D (″)	Codes
		0.1	0.3	0.6			
#1a	1 Central	✓	✓	✓	10	½	KM$_1$ID$_{0.5}$FR$_{10}$
#1b	2 Central	✓	✓	✓	10	½	KM$_2$ID$_{0.5}$FR$_{10}$
#2a	1 Central	✓	✓	✓	10	1	KM$_1$ID$_1$FR$_{10}$
#2b	2 Central	✓	✓	✓	10	1	KM$_2$ID$_1$FR$_{10}$
#3a	1 Central	–	✓	–	25	1	KM$_1$ID$_1$FR$_{25}$
#3b	2 Central	–	✓	–	25	1	KM$_2$ID$_1$FR$_{25}$
#4a	1 Wall	–	✓	–	25	1	KM$_1$ID$_1$FR$_{25W}$
#4b	2 Wall	–	✓	–	25	1	KM$_2$ID$_1$FR$_{25W}$

Size	Re		
	$v=0.1$ m s^{-1}	$v=0.3$ m s^{-1}	$v=0.6$ m s^{-1}
½″	20	91	245
1	26	150	394

Instruments) equipped with a 40 mm diameter 2° steel cone. As shown previously (Alberini et al., 2014), both fluids were found to be well represented by the Herschel-Bulkley model over a range of shear rates, $\dot{\gamma}$, from 0.1–1000 s^{-1}. The calculated rheological parameters are given for both fluids, together with polymer concentration and pH, in Table 1. The two fluids were chosen so that the effect of injection of a more viscous secondary flow, the core focus of this work, could be studied. The less viscous fluid (fluid 1) was always used as the primary flow, whilst either fluid 1 or the more viscous fluid 2 were used as the secondary flow.

A baseline superficial velocity of $v=0.3$ m s^{-1} was taken for all experiments, corresponding to a total volumetric flow rate of 180 L h^{-1} at the 1/2″ scale and 600 L h^{-1} for the 1″ scale. On the basis of these requirements, four different experiments were performed, as shown in Table 2, with the core effect of changing viscosity ratio being carried out for each experiment.

The effect of system and fluid parameters upon the blending of shear-thinning fluids were investigated starting with the effect of superficial velocity for the ½″ mixer in experiment #1 and for the 1″ mixer in experiment #2. The effect of scale can thus be examined by comparing experiments #1 and #2. Similarly the effect of flow ratio can be examined by comparing experiments #2 and #3 and the effect of inlet injection position by comparing experiments #3 and #4 (Table 3).

2.3. PLIF Measurements

Full details of the 2-D PLIF measurement and calibration methods are given in Alberini et al. (2014) and they are

Table 3
Experimental values of pressure drop for both mixer scales.

Superficial velocity v (m s^{-1})	Pressure drop ΔP (Pa) D=1/2″	Pressure drop ΔP (Pa) D=1″
0.1	1200	750
0.3	2800	1800
0.6	6700	4500

summarised below. The 2-D PLIF measurements were performed using a TSI PIV system (TSI Inc, USA) comprised of a 532 nm Nd-Yag laser (New Wave Solo III) pulsing at 7 Hz at a laser power of 15 mJ/pulse, synchronized to a single TSI Powerview 4 MP (2048×2048 pixels^2) 12 bit frame straddling CCD camera using a synchroniser (TSI 610035) attached to a personal computer. The PIV system was controlled using TSI Insight 4G software. Although the system is designed for PIV measurements, it was easily adapted for PLIF by taking the first frame of each image pair acquired by the frame straddling camera and using these images for subsequent PLIF analysis.

The system was calibrated at fixed constant laser power (15 mJ/pulse) by filling the entire pipe volume with solutions of fluid 1 (primary flow) and fluid 2 (secondary flow) fully mixed with Rhodamine 6 G dye at three different concentrations (0.1 mg L^{-1}, 0.5 mg L^{-1} and 1 mg L^{-1}). A pixel by pixel calibration was then performed using MATLAB for each concentration which confirmed a proportional relationship between the dye concentration and the measured grayscale value over this range. At low concentrations, no discernible difference in the calibration was observed whether fluid 1 or fluid 2 were used. The dye concentration in the secondary flow was thus fixed at 0.5 mg L^{-1}to ensure that the measurable concentrations for $X > 60\%$ (used the later analysis) at the mixer outlet were within this linear range. Thus the effect of the pH and concentration of the solutions upon the calibration can be ignored.

The camera is equipped with a 545 nm cut-off filter to eliminate reflected laser light so that only the fluorescent light emitted by the dye ($\lambda=560$ nm) excited in the measurement plane is captured on the image. The spatial resolution of the measurements was 10 µm pixel^{-1} and 20 µm pixel^{-1} for the ½″ and 1″ scale mixers respectively.

To assess the possibility of temporal variation between images taken at the same flow conditions, ten images were acquired in three batches spaced several minutes apart for each experiment. No variation was observed in any of image batches, or between batches, taken at the same flow conditions. This was expected due to laminar regime of the system which allows the pattern to be consistent over the time. Therefore the subsequent analysis was performed for each experiment using a single image.

3. Analysis of PLIF images

Processing of the PLIF images was carried out using the MATLAB software package (Mathworks Inc, USA). The 12 bit images were imported into MATLAB and converted into a 2048 × 2048 matrix with each element in the matrix corresponding to a pixel in the image: each element contains an integer number between 0 (black) and 4095 (white). The region within the matrix corresponding to the pipe cross section was isolated and the number of elements (pixels) in this region, N, was counted.

3.1. CoV and maximum striation area

The CoV was then determined using Eq. (1), defining the mixing property, C_i, as the concentration in each pixel (proportional to the grayscale value). To determine the maximum striation area, an algorithm was used which counts the number of contiguous pixels on a row-by-row basis with the same grayscale value (within a pre-defined tolerance) and thus within the same striation. If the next pixel is outside the defined tolerance, the counter is reset to zero and the next striation is thus identified. The procedure repeats until the entire image area is read. The distribution of striation areas in terms of numbers of pixels thus obtained is converted to a (length scale)^2 from the image calibration and the area of the largest striation is thus identified. The maximum striation areas are then normalised by the whole cross section of the static mixer. In this work, the tolerance used was a 5% relative difference in terms of grayscale value to identify a border between different striations. As this algorithm works on a row-by-row basis, striations spanning more than one row are counted more than once which weights the distribution in favour of the larger striations, since they occupy a larger cross sectional area. Although these data are not therefore absolute, the method does allow relative comparisons between the different experiments and avoids the need for manually intensive analysis. It should be noted that this method identifies the largest striation regardless of its concentration.

3.2. Areal distribution method

An outline of the areal distribution method is given here, for full details please refer to Alberini et al. (2014). A typical raw image obtained from PLIF is shown in Fig. 2a. A complex asymmetric distribution of striations are observable and it is clear that not all the striations contain the same concentration of fluorescent dye, since they possess a range of grayscale values from black to white. This richness within the data is not captured by calculation of CoV or maximum striation area method, since the concentration is not considered as a function of the striation size or shape.

The analysis proceeds by calculation of the mean value of grayscale in the image, $\overline{G}$, which is proportional to the fully mixed concentration, $\overline{C}$. Assuming plug flow, the mass balance of dye from the inlet to the PLIF measurement point can then be checked assuming that the plug flow does not drastically affect the grayscale values in the selected cross section.

$$\overline{G} = \frac{F_1 G_1 + F_2 G_2}{F_1 + F_2}, \tag{2}$$

where F_1 and F_2 are the volumetric flow rates of the primary and secondary flows respectively and G_1 ($G_1 \rightarrow 0$) and G_2 are the grayscale values corresponding to the concentrations of dye present. The theoretical values for $\overline{G}$ calculated using Eq. (2) were within 5% of the experimentally determined values, thus the mass balance was closed to within an error of ±5% for all experiments.

Then X is defined as a percentage of this fully mixed value $\overline{G}$ with $X=100\%$ for $G=\overline{G}$. Considering, as an example, $X=95\%$ and assuming the plug flow mass balance closes, this can correspond to a pixel containing either $(1.05 \, F_1 + 0.95 \, F_2)$ or $(0.95 \, F_1 + 1.05 \, F_2)$.
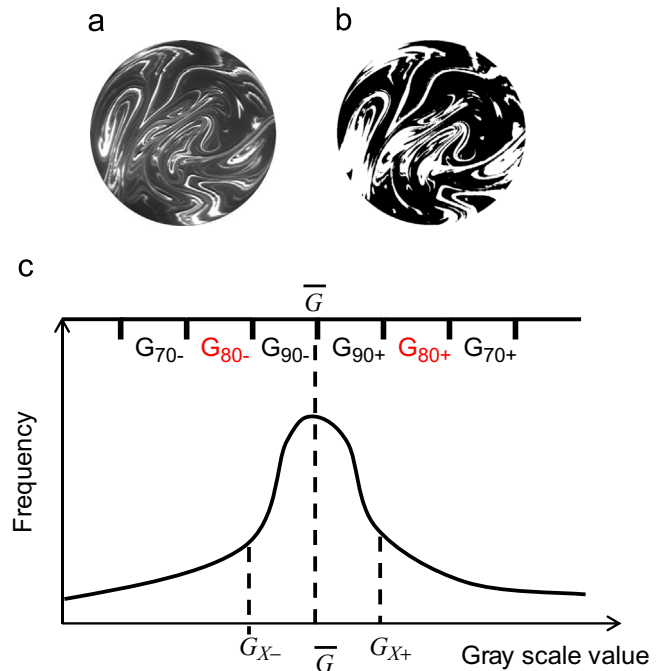

Fig. 2. (a) Example concentration distribution of the secondary flow obtained using PLIF across the pipe cross section past the mixer outlet; (b) binary image showing application of the areal distribution method with pixels with a level of mixedness $X > 90\%$ shown in white; and (c) schematic of frequency distribution of grayscale values, related to the level of mixedness, X.

Both pixels would of course possess the same CoV from eq. (1). Thus a value of mixing $> X\%$ has an upper and lower bound defined by X_- and X_+. The lower and upper limits of grayscale value for each level are then simply obtained as: $G_{X-} = [1-(1-X)] \, \overline{G}$ and $G_{X+} = [1+(1-X)] \, \overline{G}$ since $G_2 = 0$. So for example using Eq. (2) if $X = 95\%$ mixing, $G_{X-} = 0.95\overline{G}$ and $G_{X+} = 1.05\overline{G}$.

Using MATLAB and the freeware image analysis tool Image J (http://rsbweb.nih.gov), the pixels in the image are sorted into bins which correspond to $G_{X(i+1)-} < G < G_{X(i)-}$ and $G_{X(i)+} < G < G_{X(i+1)+}$, centred at $G_{X(i)-} = G_{X(i)+} = \overline{G}$ (when $i=0$) enabling generation of a histogram. Thus corresponding to a level of mixedness of $X > 90\%$: this arbitrary region is shown in Fig. 2b where the pixels in range are set to white ($G=4095$) in the image, with the remaining out of range pixels being set to black ($G=0$). By repeating this procedure over a range of values of X, both discrete and cumulative areal distributions of mixing intensity are thus obtained. A schematic of a typical frequency distribution is shown in Fig. 1c; note that the distribution can be asymmetric, as discussed in Alberini et al. (2014).

3.3. Individual striation method.

The identification of individual striations, later focussing on those with high values of X, is obtained using a MATLAB script which utilises both the MATLAB image processing toolbox and the DIPimage toolbox developed by the Quantitative Imaging Group at TU Delft (http://www.diplib.org). The image analysis scripts used in this work are available by contacting the corresponding author.

The script performs the following key operations, the initial parts being similar to the areal distribution method. Firstly the image is imported in MATLAB and a circular mask is created to identify the region of interest (e.g. as shown in Fig. 2a). Using the value of $\overline{G}$, the levels of mixing intensity, X, per pixel, are evaluated as before. Then the ranges of X are defined and for each range, two images are created by MATLAB where only the striations in the range of interest are shown: the first shows all the striations in the range of G_{X-} and the second shows all the striations for G_{X+}. The next step is to label the
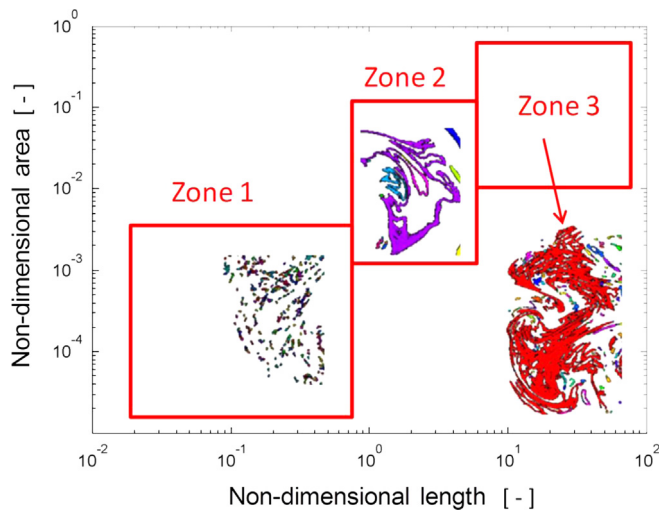
Fig. 3. Zonal representation of the individual striation method. The striations are classified according to three different zones that describe the size of striation in terms of no dimensional area and perimeter.

striations for each created image using the command 'label' from the DIPimage toolbox. The minimum size of a striation is in the order of 4 pixels. The final step, after the detection of the striations with a selected range of mixing intensity, is the evaluation of their corresponding areas and perimeters. These features are evaluated using the command 'measure' from the DIPimage toolbox which produces a matrix where the columns are the number of detected objects on the image and different rows correspond to different measurements. Using this command only two of the multiple options are used: they are 'size' for the area and 'Perimeter' for the perimeter.

In this analysis the ranges of mixing intensity used were the same as those in the areal distribution method: further analysis was focussed on the two ranges where the intensity is the highest ($X > 90\%$ and $80 < X < 90\%$). The data obtained for these ranges were plotted in the form of a graph presented in Fig. 3. The y axis is the area of each striation non-dimensionalised by dividing by the cross sectional area of the pipe; whilst the x axis is the perimeter of each striation non-dimensionalised by dividing by the perimeter of the injected secondary flow. Note that this analysis is focussed only on mixing intensities, $X > 90\%$.

The graph may be divided in 3 arbitrary zones in order to compare between different experiments. These three zones were classified as

Zone 1 – characterised by striations with small non-dimensional areas (maximum $\sim 10^{-3}$ of whole cross section) and non-dimensional perimeters (maximum $\sim 10^{\circ}$ of the perimeter of the injection); if all measurements are in this zone then mixing is expected to be poor since there are a large number of well mixed small spots which are not blended into the bulk fluid.

Zone 2 – where medium size striations are located (maximum non-dimensional area $\sim 10^{-1}$ of whole cross section and maximum non-dimensional perimeter ~ 10): in this group all the striations typical of lamellar structures are included.

Zone 3 – characterised by very large striations, in this case since X is very high this corresponds to good mixing performance across the majority of the pipe cross section.

4. Results and discussion

Fig. 4 shows raw PLIF images obtained for each experiment across the pipe cross-section just downstream of the mixer outlet. When fluid 1 is used as the secondary flow, Fig. 4a shows that the
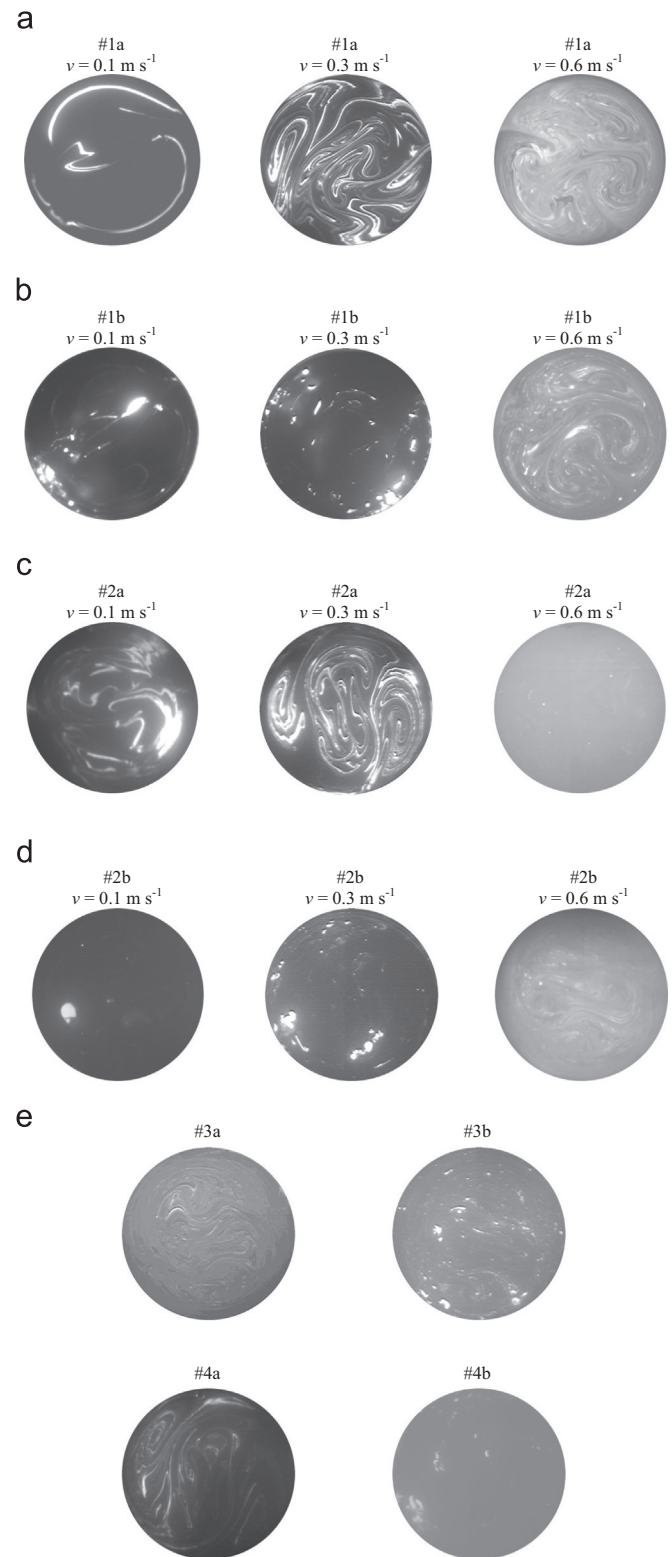

Fig. 4. Raw PLIF images obtained from all experiments: (a) Experiment #1a at each superficial velocity; (b) Experiment #1b at each superficial velocity; (c) Experiment #2a at each superficial velocity; (d) Experiment #2b at each superficial velocity; (e) Experiments #3 and #4 at the base velocity of 0.3 m s^{-1}. Full details of experimental conditions are given in Table 2.

pattern of striations radically changes with increasing superficial velocity for experiments carried out using the ½″ static mixer (#1a), as would be expected. At lower velocities, the dye is concentrated in a few striations whilst at higher velocities, the

number of striations is observed to increase. Similar behaviour is observed at the 1″ scale (#2a), shown in Fig. 4c; comparing both scales the PLIF images show the effect of stretching and folding due to the geometry of the mixer elements. As the mixing performance increases, the difference between grayscale values in different striations decreases drastically: without proper image analysis it is impossible to detect any difference in grayscale values by eye in the cross section. For example, the differences in values of grayscale across the image are of the order of 10 in Fig. 4c at $v = 0.6 \text{ m s}^{-1}$.

Switching the secondary flow to fluid 2 illustrates the dramatic effect of changing viscosity ratio. Completely different patterns are observed in the images obtained for experiments #1b and #2b shown in Figs. 4b and 4d respectively. The presence of fluid 2 causes the formation of viscous unmixed threads identified by spots on the images. As the velocity increases the spots initially decrease in size, then the filaments become less prevalent and striations appear as the velocity increases further. The observed patterns for the experiments performed at the base velocity of $v = 0.3 \text{ m s}^{-1}$ (#1b, #2b and #3b) are similar but the experiment carried out with the higher flow ratio (#3b) is characterised by the presence of a greater number of smaller spots.

Experiments carried out with injection of the secondary flow at the wall (#4a and #4b) shown in Fig. 4e demonstrate completely different mixing patterns compared to similar experiments carried out with central injection (#3a and #3b). For wall injection the dyed fluid is concentrated only on half of the cross section, demonstrating very poor radial mixing of the secondary flow.

4.1. Effect of velocity and scale at constant flow ratio

The effects of superficial velocity and injected fluid rheology as a function of mixer scale have been examined initially by calculation of CoV as a function of energy input per unit mass, the latter being a useful quantity as it reflects the required energy input to a process to achieve a required mixing duty. Values of CoV versus $\Delta P / \rho$ are shown in Fig. 5a; they were determined for both ½″ and 1″ devices for both injected fluids (#1 and #2) at each of the three different superficial velocities used.

Notable differences are observed between each experiment, unsurprisingly increasing $\Delta P / \rho$ gives a much improved mixing performance. Use of the more viscous fluid 2 as a the secondary flow causes a worse mixing performance; a remarkable exception is observed when comparing values of the CoV between experiment #1a and #1b at the lowest measured velocity. This is may be due to the limitation of the CoV method which does not distinguish the differences when the system is highly heterogeneous, only a few large unmixed striations are observed in the PLIF images in Figs. 4a and 4b. For both ½″ and 1″ mixers, the general trend is similar, with CoV decreasing with increasing energy input to the system. The values of CoV in Fig. 5a are very similar when experiments #1a to #2a and #1b to #2b are compared, though generally the 1″ device performs slightly better when fluid 2 is used as the secondary flow; results when fluid 1 is used are indistinguishable between the scales, apart from at very low $\Delta P / \rho$.

In terms of maximum striation area (Fig. 5b), inconsistent trends in behaviour are shown for both the ½″ experiments (#1a) and (#1b) and 1″ experiments (#2a and #2b). As the energy per unit mass increases with velocity, the maximum striation area increases for #1a yet decreases for #1b. This phenomenon may occur because the mixing of non-Newtonian fluids does not involve a symmetric lamellar structure; the raw images in Fig. 4 show the generation of many large zones of poor mixing. This is a good example of how the evaluation of mixing performance based upon a single criterion can create misleading or uncertain results, since these trends are not consistent with the CoV shown
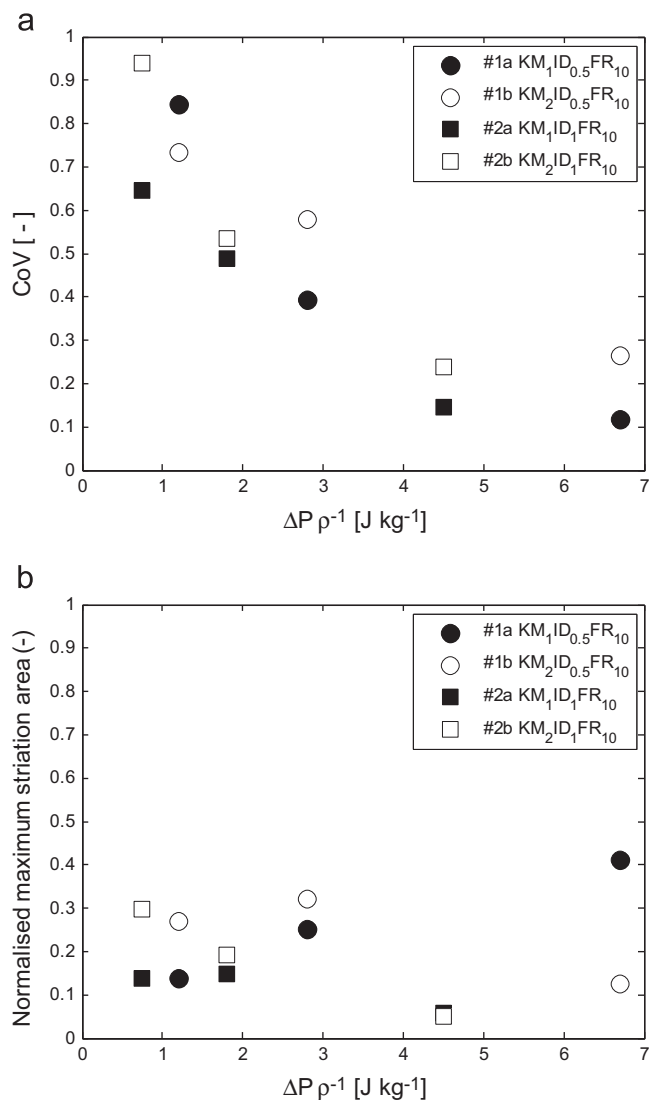
Fig. 5. Mixing performance as a function of energy input per unit mass ($\Delta P / \rho$) for #1 and #2: (a) CoV (intensity of segregation); and (b) max striation area (scale of segregation).

in Fig. 5a. For the 1″ experiments (#2a and #2b), the trend of maximum striation area is also unclear, but at both scales the injection of fluid 2 gives greater maximum striation thicknesses apart from at the highest energy input for experiment #1 (again this is a factor of the heterogeneity of the mixing at these conditions as shown in Fig. 4). Although these inconsistent results may be due in part to the behaviour of the Herschel Bulkley fluids used, the issue is that the criteria in Fig. 5 cannot be used reliably across the range of fluids used in industrial practice, which includes non-Newtonian fluids. Though a general conclusion may be extrapolated from this introductory analysis, a deeper approach is needed to classify and compare different experiments with such complex patterns in a consistent way. This has been carried out in the rest of this paper using the areal distribution and individual striation methods.

Fig. 6 shows the distribution of area fraction as a function of level of mixedness, X, from the areal distribution method for experiments #1 and #2. As expected the fraction for $X > 90\%$ increases with increasing velocity for each experiment, almost at the same rate as $X < 60\%$ decreases. Fig. 6a shows the divergences between experiment #1a and #1b are clear in terms of absolute fraction values of X, where the experiment with fluid 1 as the
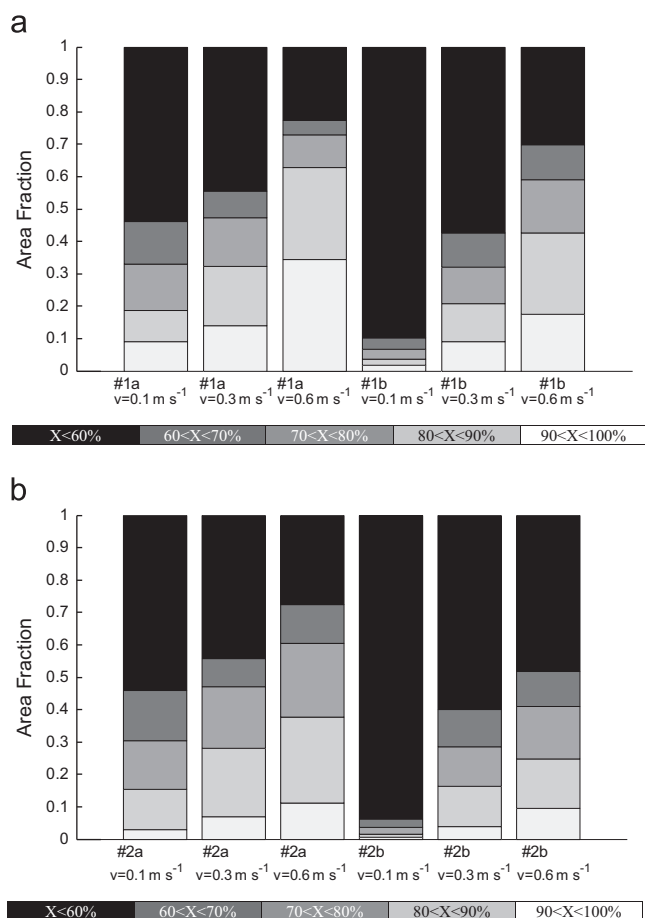
Fig. 6. Bar graph showing discrete areal intensity distributions (a) for #1 and (b) for #2 at each superficial velocity.

Fig. 7. Area fraction $X > 80\%$ from areal distribution method versus energy input per unit mass ($\Delta P/\rho$) for experiments #1 and #2.

secondary flow (#1a) always performs better than when fluid 2 is the secondary flow (#1b). Whilst the previous analysis showed a lower value of CoV for #1b at the lower velocity in Fig. 5a, this approach shows a much poorer expected mixing performance, with most of the pixels having a value of $X < 60\%$. This suggests that this approach is more robust for analysis of highly heterogeneous mixing fields. The effect of increasing velocity is strongest in experiment (#1b), this is particularly observable by comparing the experiments at $v = 0.1$ m s^{-1} and at $v = 0.3$ m s^{-1} where the fraction with $X > 90\%$ becomes over 4 times larger.

Fig. 6b shows the distribution of area fraction as a function of level of mixedness for the ½″ experiments (#2). The general trends are similar to the ½″ experiments but the absolute values for different levels of X are different. Increasing the velocity increases the area fraction for $X > 90\%$ as expected, almost proportional to the velocity. Comparing Fig. 6a with Fig. 6b, as expected the fraction of $X > 90\%$ is higher with the fluid 1 as the secondary flow at both scales, but is doubled for the ½″ mixer when compared to the 1″ mixer. The presentation of data using this method predicts that the overall best performance (in terms of area fraction for $X > 90\%$) is for the ½″ static mixer, which is slightly better than the 1″ mixer. However, if $X > 80\%$ is chosen as the criterion, the data appear independent of scale. The choice of values of X for comparison should be dictated in practice by the requirements of the downstream process which is an advantageous property of the areal distribution method.

Fig. 7 provides a general overview of the performance as determined by the areal distribution method as function of energy per unit mass. The area fraction plotted on the ordinate is for
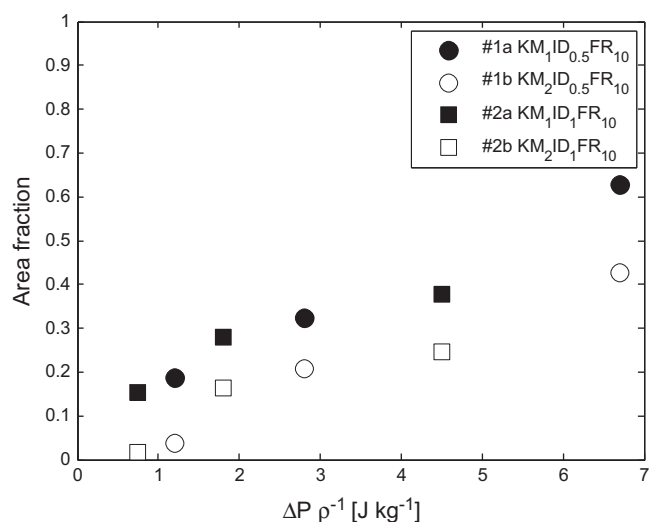
mixing intensity, $X > 80\%$, confirming that the mixing performance appears to be independent of the size of static mixer if this criterion is used. Referring to Figs. 6a and 6b, the plotted points are thus the sum of the first two area fractions for the highest ranges of X. Increasing energy input per unit mass increases the area fraction for $X > 80\%$ for both systems regardless of which fluid is used as the secondary flow, nevertheless a worse performance is observed overall when fluid 2 is used.

Images of the striations detected by the individual striation method are shown for $X > 90\%$ and $80 < X < 90\%$ in Figs. 8 and 9 for the ½″ and 1″ mixers respectively at each superficial velocity. The data illustrate the effect of scale and changing viscosity ratio by using either fluid 1 or fluid 2 as the secondary flow. The different striations detected by the MATLAB script are identified with different colours. Due to the high number of striations present in the images the same colour may be repeated in different striations. Figs. 8 and 9 also show the striations classified according to the zonal representation illustrated in Fig. 3 for $X > 90\%$.

Fig. 8 shows the shape of the striations for experiment #1; if unpicked pixels are located inside the coloured striation, the algorithm does not count this in the evaluation of total striation area. Visual examination of Figures 8ai, 8bi and 8ci reveals that both the number and area of striations increases considerably with increasing superficial velocity from 0.1 to 0.3 to 0.6 m s^{-1} respectively, due to increasing the energy input to the system. This is observed with use of either fluid 1 or fluid 2 as the secondary flow; at the same fixed velocity the number of striations observed is much less for fluid 2 than fluid 1 until the highest superficial velocity is reached. The pictures for X_- and X_+ show the different striations for the upper and lower bound of the selected ranges of level of mixedness, X, as described in §3.3. Notable changes in the striation shapes occur as the velocity increases: the energy of the system drastically affects the spreading of the secondary flow by increasing the size and swirl of the striations. The largest striations are found mostly at the wall, where the shear magnitudes are highest and local residence times are longest. For experiment #1b (where fluid 2 forms the secondary flow), Fig. 8a(i and ii) shows that at $v = 0.1$ m s^{-1} and 0.3 m s^{-1} respectively, the detected striations are only concentrated around the spots where the dye is unmixed. The fluids used possess a Herschel Bulkley rheology, thus exhibiting both a yield stress and shear thinning behaviour. It is possible that the yield stress imposes a limitation on the

swirling generated by the static mixer elements at lower velocities limiting the spreading of dye around the cross section. When the velocity increases further up to $v=0.6$ m s^{-1}, the possible effect of

yield stress on the formation of striations would be lessened, potentially due to higher shear stresses present in the flow and also it seems that the geometry induces a rotational component to
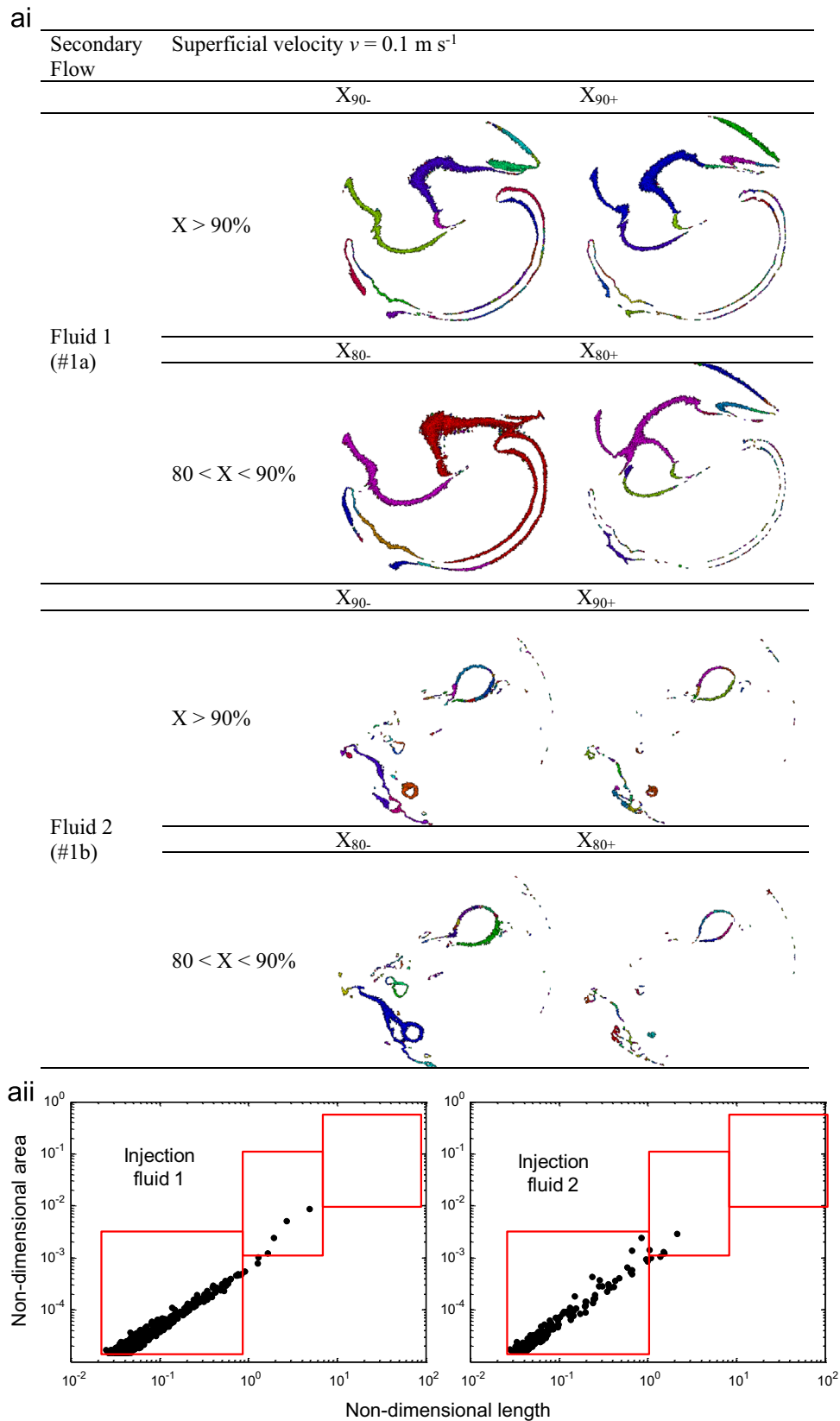

Fig. 8. Illustration of striations detected using the individual striation method for selected ranges of level of mixedness, X, for experiment #1 using the ½″ mixer at (a) $v=0.1$ m s^{-1} – (ai) visualisation of striations (aii) zonal representation; (b) $v=0.3$ m s^{-1} – (bi) visualisation of striations (bii) zonal representation; (c) $v=0.6$ m s^{-1} – (ci) visualisation of striations (cii) zonal representation.

bi

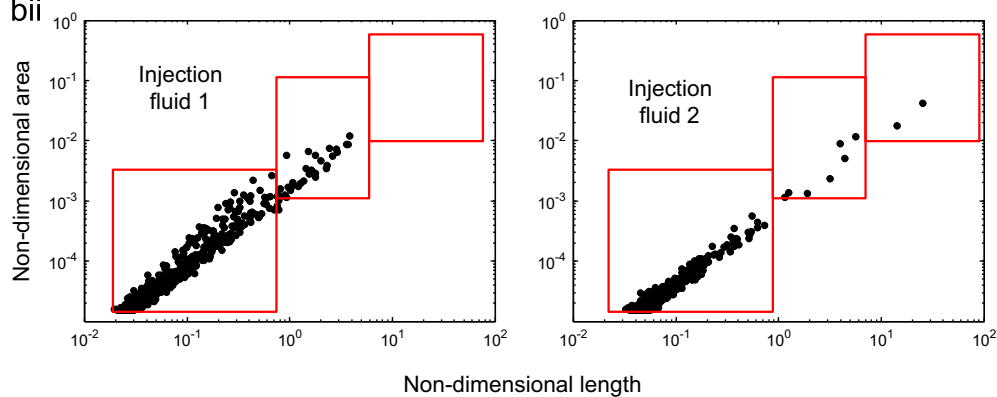| Secondary Flow	Superficial velocity $v = 0.3\ \mathrm{m\ s^{-1}}$	
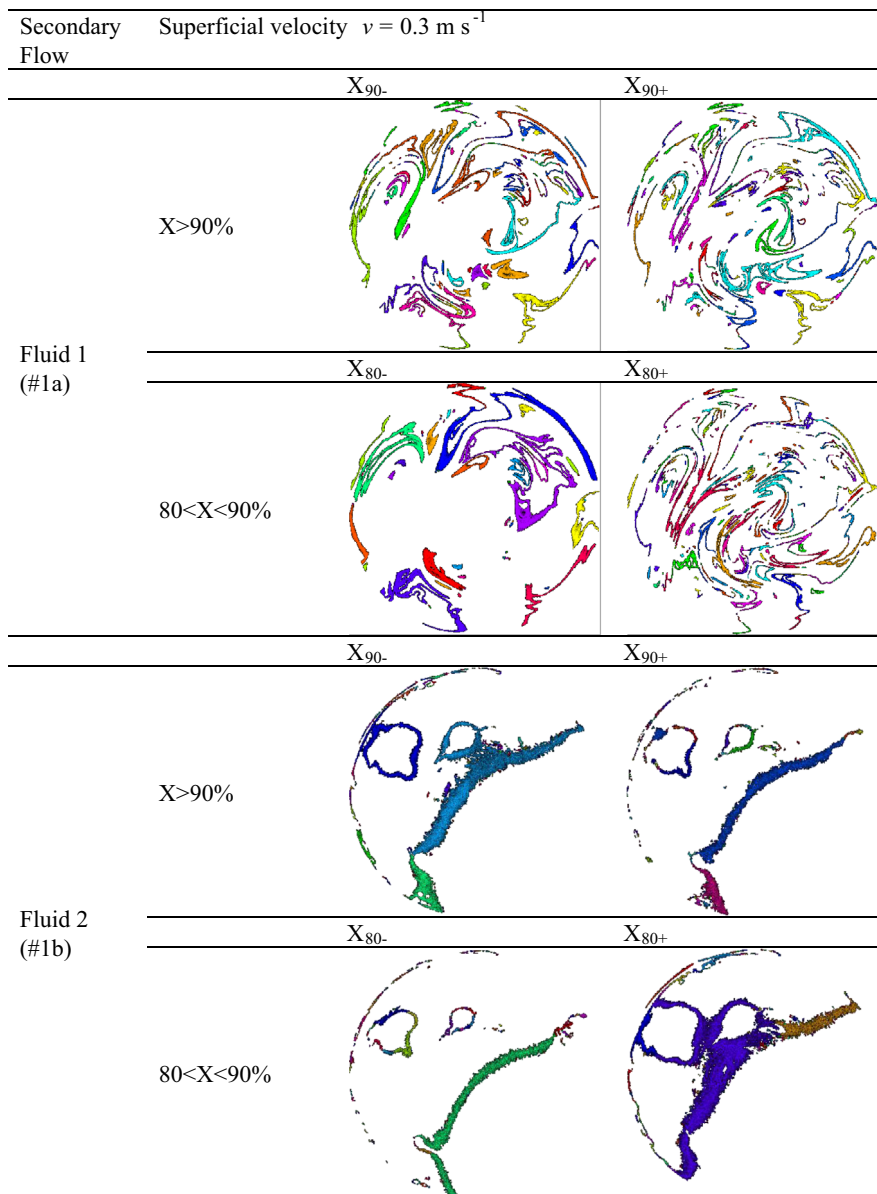
Fig. 8. (continued)

the fluid motion that drastically increased the level of mixedness. It should be noted that the ideal mixing situation would be a single uniform striation occupying the total cross sectional area of the mixer with a level of mixedness of $X=100\%$.

The zonal representation of striation size distribution is shown for superficial velocities, $v=0.1$, 0.3 and $0.6\ \mathrm{m\ s^{-1}}$ in Fig. 8a(ii), b(ii) and c(ii) respectively for $X>90\%$ (X_{90-} and X_{90+}). At $v=0.1\ \mathrm{m\ s^{-1}}$, the lowest velocity, the points are concentrated

ci

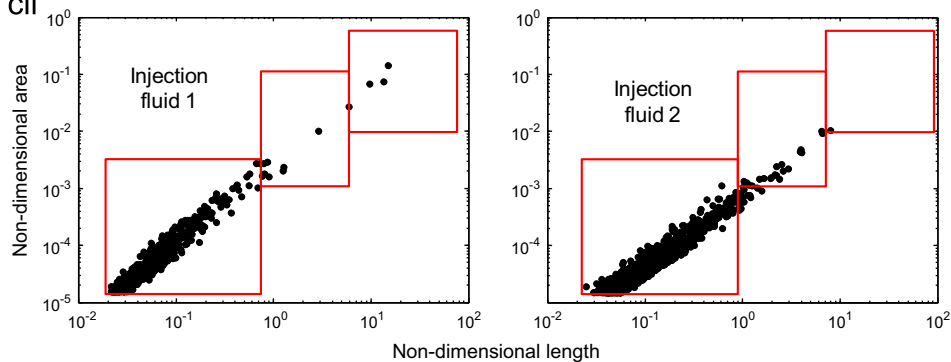| Secondary Flow	Superficial velocity $v = 0.6$ m s^{-1}	
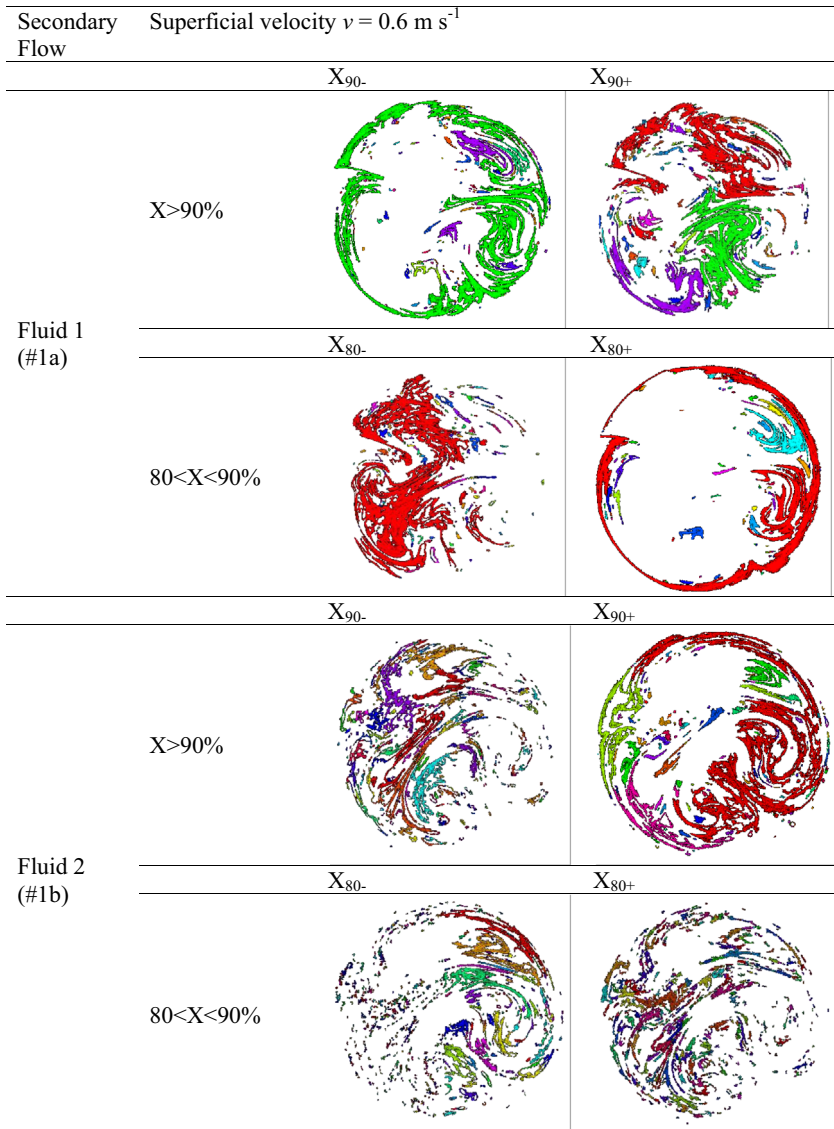
Fig. 8. (continued)

in zone 1 (referring to Fig. 3) underlining the presence of small well mixed regions which are not incorporated with the poorly mixed bulk fluid - leading to poor mixing. At the intermediate velocity of $v=0.3$ m s^{-1} the number of points in zone 1 decreases whilst zone 2 becomes more populated; the total number of points also increases. A few isolated larger striations are observable in zone 3 for fluid 2. At the highest velocity of $v=0.6$ m s^{-1} the total number of points again increases, but the spread is

shifted towards zones 2 and 3 due to the presence of larger striations due to the increased stretching and swirling of the fluid elements. The presence of points in zone 3 in this case is an indication of improved mixing; since these larger striations contain well mixed fluid ($X > 90\%$). Again, it is notable that when fluid 2 is used as the secondary flow, the illustration would indicate a poorer mixing performance as the data are more clustered towards the bottom left hand corner of the graph,

and generally fewer in number, apart from a few isolated larger striations observable in Fig. 8b(ii).

Fig. 9 shows an identical presentation of the individual striation method for experiment #2 where the 1″ KM static mixer device was used. For the experiments run at the lowest velocity of $v = 0.1$ m s^{-1} (Fig. 9a), the number of striations is similar to the ½″ experiments for use of both fluid 1 and fluid 2 as the secondary flow. Comparing the two scales, further similarity is seen in the increasing elongation of the striations with increasing velocity and again, use of fluid 2 as the secondary
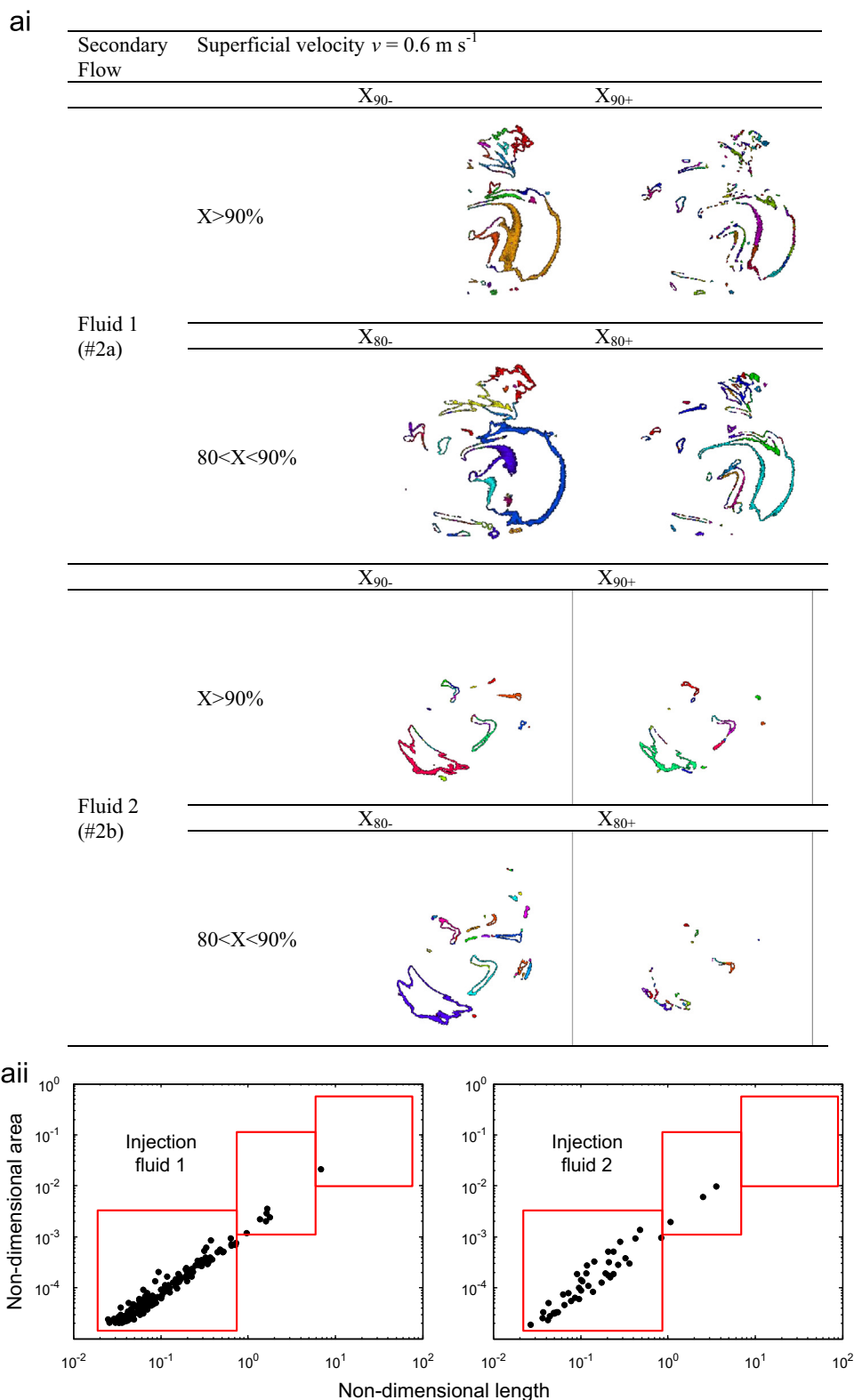

Fig. 9. Illustration of striations detected using the individual striation method for selected ranges of level of mixedness, X, for experiment #2 using the 1″ mixer at (a) $v = 0.1$ m s^{-1} – (ai) visualisation of striations (aii) zonal representation; (b) $v = 0.3$ m s^{-1} – (bi) visualisation of striations (bii) zonal representation; (c) $v = 0.6$ m s^{-1} – (ci) visualisation of striations and (cii) zonal representation.

bi

Secondary Flow	Superficial velocity $v = 0.3$ m s^{-1}	
	X_{90-}	X_{90+}

Fluid 1 (#2a)	X_{80-}	X_{80+}

	X_{90-}	X_{90+}

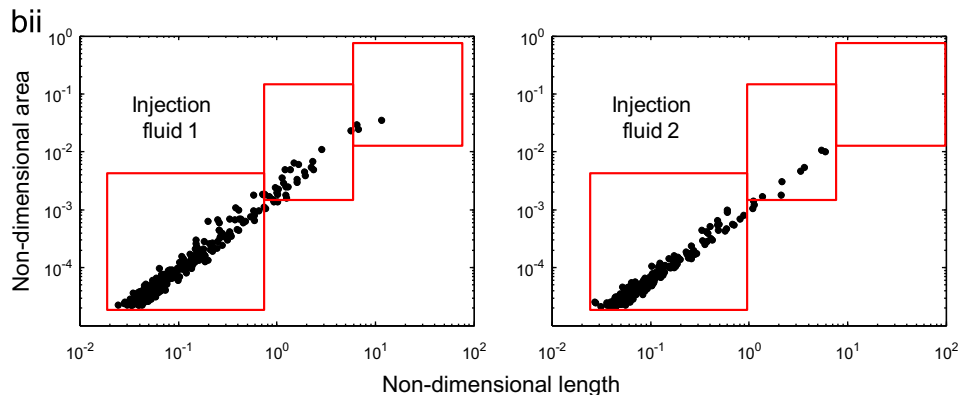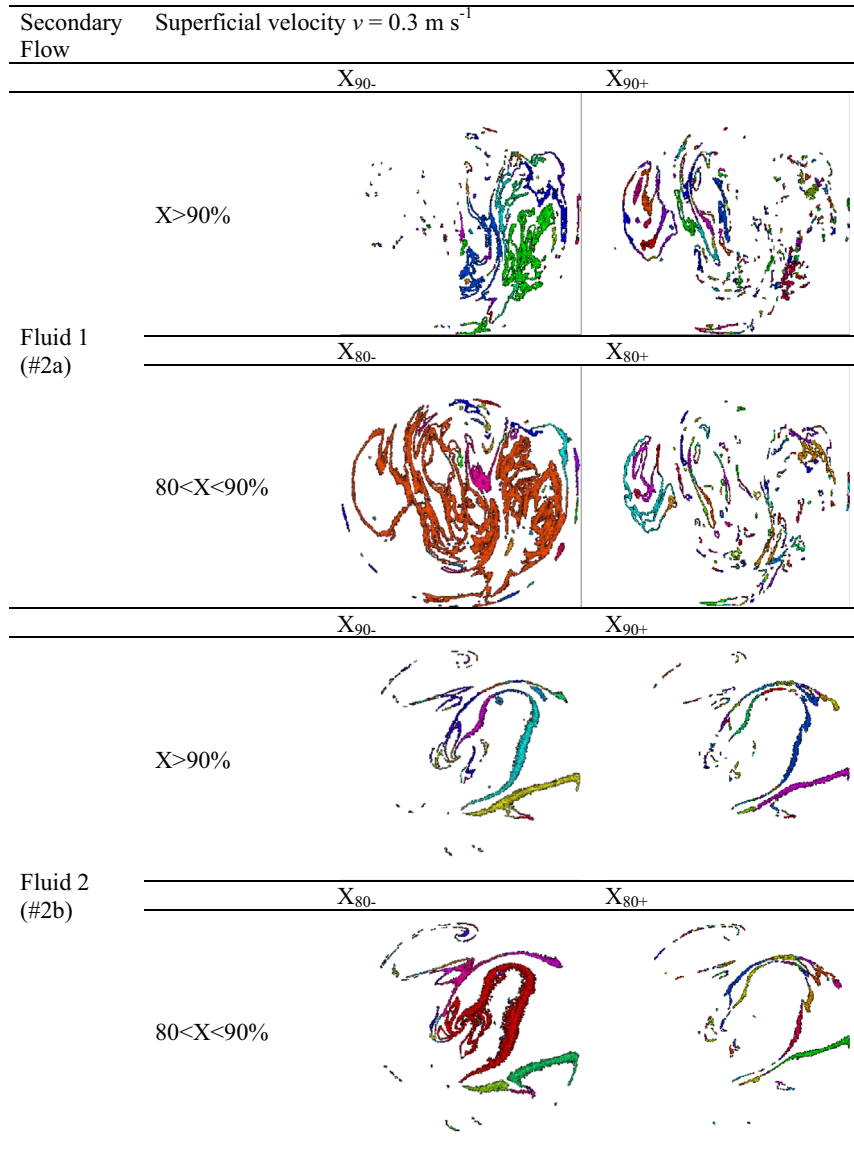| Fluid 2 (#2b)	X_{80-}	X_{80+}

bii

Fig. 9. (continued)

flow limits the swirling and spreading of the dye. However, the shape of the striations and how they are distributed across the pipe cross-section is noticeably different between scales, in particular there are a larger number of larger striations for the lower bound (X-) that were not evident in the ½″ mixer experiments.

The zonal representation follows a similar pattern, with larger striations observable as the superficial velocity is increased. Referring to Fig. 9a(ii), b(ii) and c(ii) the general trend is similar to that seen in the previous set of experiments for ½″. The points of the graphs are concentrated mainly in zone 1 when poor mixing affects the system, at lower velocity. Increasing the energy in the

ci

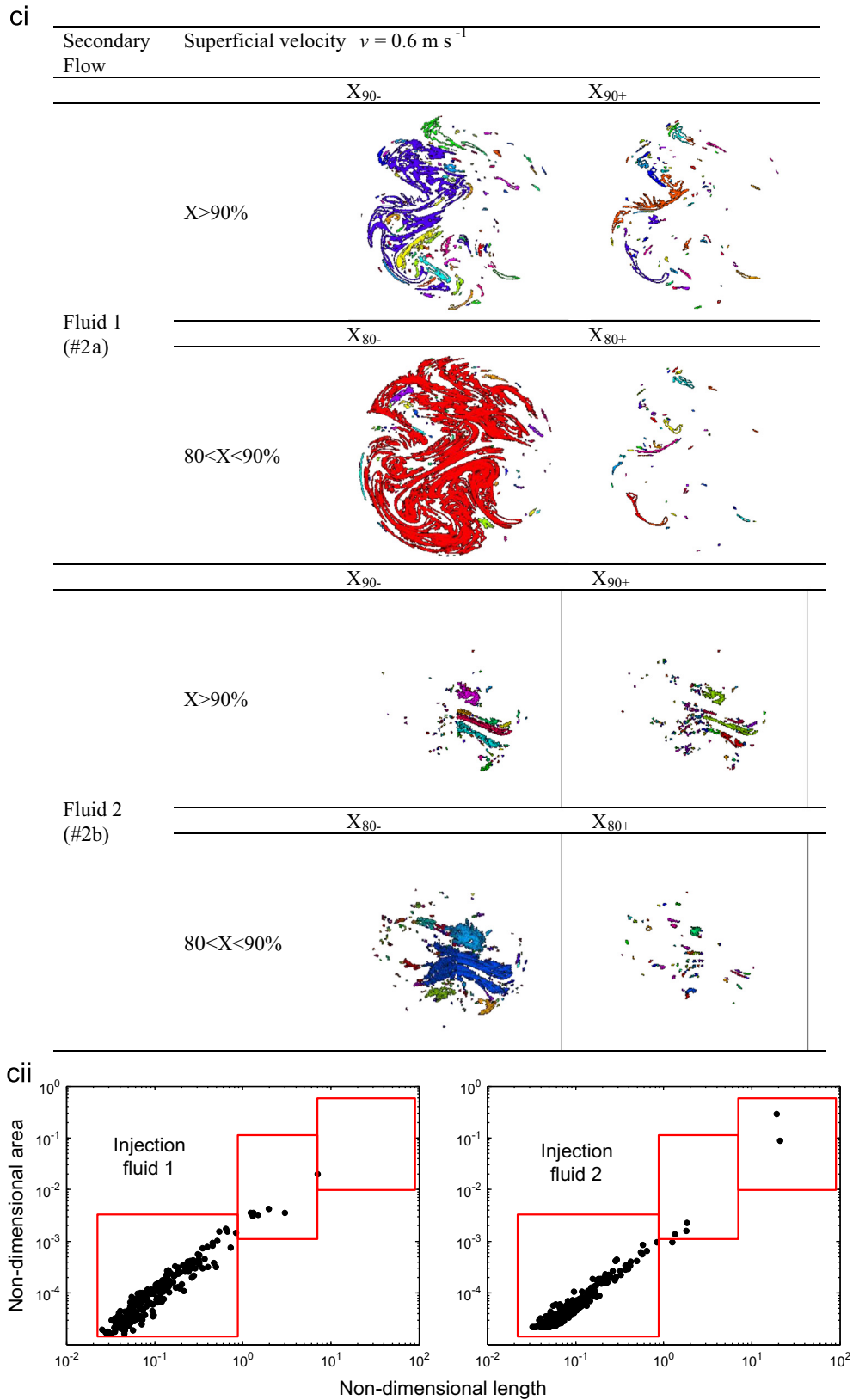| Secondary Flow	Superficial velocity $v = 0.6$ m s^{-1}	

Fig. 9. (continued)

system the mixing improves, the number of points increases and the size of striations increase which is highlighted by the presence of points in zone 3, indicative of high mixing performance. Clearly, the use of fluid 2 as the secondary flow has a strong effect on the

striations distribution limiting the number of points in zone 2 and 3 for superficial velocities of 0.1 and 0.3 m s^{-1} (Fig. 9a(ii), b(ii)).

The zonal representation demonstrated above enables the identification of poor mixing in terms of the distribution and size
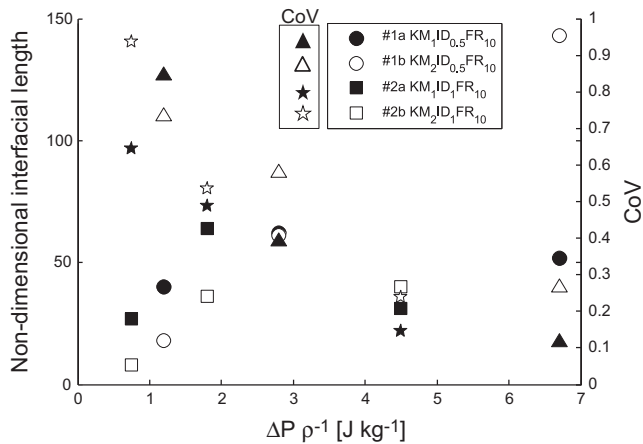
Fig. 10. Total interfacial length from the individual striation method normalised by the perimeter of the injected fluid for levels of mixedness, $X > 80\%$ versus energy input per unit mass ($\Delta P / \rho$) for experiments #1 and#2.

of the 'well-mixed' striations. A striation pattern with a poor structure is indicated by a large number of zone 1 striations, which corresponds to spots of well mixed fluid which are not incorporated into the bulk fluid; this is indicative of poor mixing. Conversely, presence of striations in zone 3 indicates large regions of the cross-section which are well-mixed. The analysis of the striation distribution gives a measure of the consequences of different flow conditions within the static mixer: with increasing velocity it seems that the geometry induces a rotational component to the fluid motion that drastically increases the level of mixedness. This phenomenon was also noticed in the flow field results obtained using PEPT by Rafiee et al. (2013). The quantification and localisation of different regions with different levels of mixedness is the key objective of this work, which gives an insight into the changes in the mixing patterns for the analysed system.

The data from the individual striation method can be summarised by calculation of the sum of all the striation perimeters for each experiment to obtain the total interface length (non-dimensionalised by the perimeter of the injection), shown in Fig. 10 for experiments #1 and #2 as a function of energy input per unit mass. The CoV data from Fig. 5 are also plotted on Fig. 10 for comparison. As expected, by increasing the energy per unit mass (superficial velocity) the total interface length initially increases for both injections due to the increased swirling motion within the mixer. Then, the trend is reversed as the number of striations decreases and their size increases. This presentation therefore needs to be treated with caution since the parameter of total interface length cannot be directly correlated to mixing performance: in this respect it similar to maximum striation area or other single lengthscale based measures. The non-Newtonian nature of the fluids, and their consequent impact upon the mixing, may also be a contributing factor.

4.2. Effect of flow ratio and injection position at constant velocity and scale

Fig. 11a shows values of CoV and maximum striation area at constant $\Delta P / \rho$ for the experiments carried out at different flow ratios (10:1 for experiment #2 and 25:1 for #3) and different inlet injection positions of the secondary flow (central injection for experiments #2 and #3 and wall injection for experiment #4, see Table 2). All of these experiments were carried out in the 1″ diameter mixer. The data show some significant differences, with wall injection performing particularly poorly (#4) whilst for central injection a flow ratio of 25 (#3) gives a better result than a flow ratio of 10, which can be attributed to less volume of secondary flow which needs to be mixed with the primary flow.
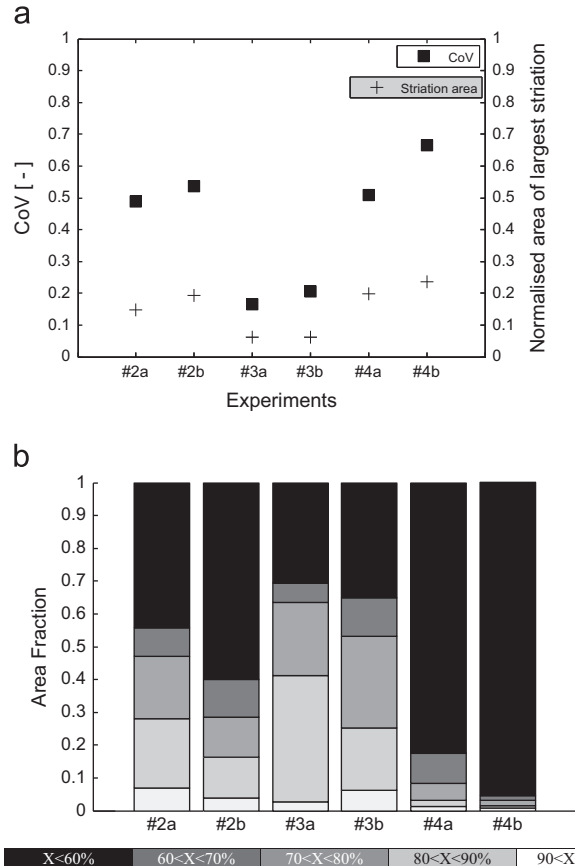
a

b

Fig. 11. Effect of flow ratio and injection position using the 1″ mixer at $\nu = 0.3 \text{ m s}^{-1}$: (a) CoV (intensity of segregation) and max striation area; (b) bar graph showing areal intensity results for experiments #2, #3, and #4.

The areal distribution method produces results which are consistent with the CoV data as shown in Fig. 11b. The effect of changing flow ratio is even more pronounced; despite the fraction of $X > 90\%$ for #3a being lower than for #2a, the fraction of mixing intensity of $X > 80\%$ is much higher for (#3a, b) than in experiments (#2a, b). Thus the experiments with a flow ratio of 25 exhibit better performance based on this criterion. It can be seen in both Figs. 11a and 11b that moving the injection position to the wall drastically reduces the mixing performance whilst all other parameters are kept constant; all the methods can detect the influence of different injection position. Fig. 11b shows a large increase in the $X < 60\%$ area fraction for experiments with wall injection (#4a and #4b) compared to central injection (#3a and #3b), whilst the area fraction is much reduced for $X > 80\%$.

The analysis from the individual striation method for experiments #3 and #4 is presented in Figs. 12 and 13. The comparison between experiments with a flow ratio of 10 (#2) and 25 (#3) may be made by comparing Fig. 9b and Fig. 12. There are notably larger number of striations for a flow ratio of 25 when fluid 2 is used as the secondary flow (Fig. 12a) compared with a flow ratio of 10 (Fig. 9b(i)), particularly for $80 < X < 90\%$. These striations are clustered in zone 1 (Fig. 12b); it noted that the mixing performance according to Fig. 11 is improved according to the areal distribution bar graph (Fig. 11b). The values of CoV would suggest a much larger improvement, but this is not borne out by the striation based analyses.

The results obtained for wall injection shown in Fig. 13 are rather dramatic, showing a general absence of striations for $X > 80\%$ regardless of whether fluid 1 or fluid 2 is used as the secondary flow. The mixing performance for experiments with
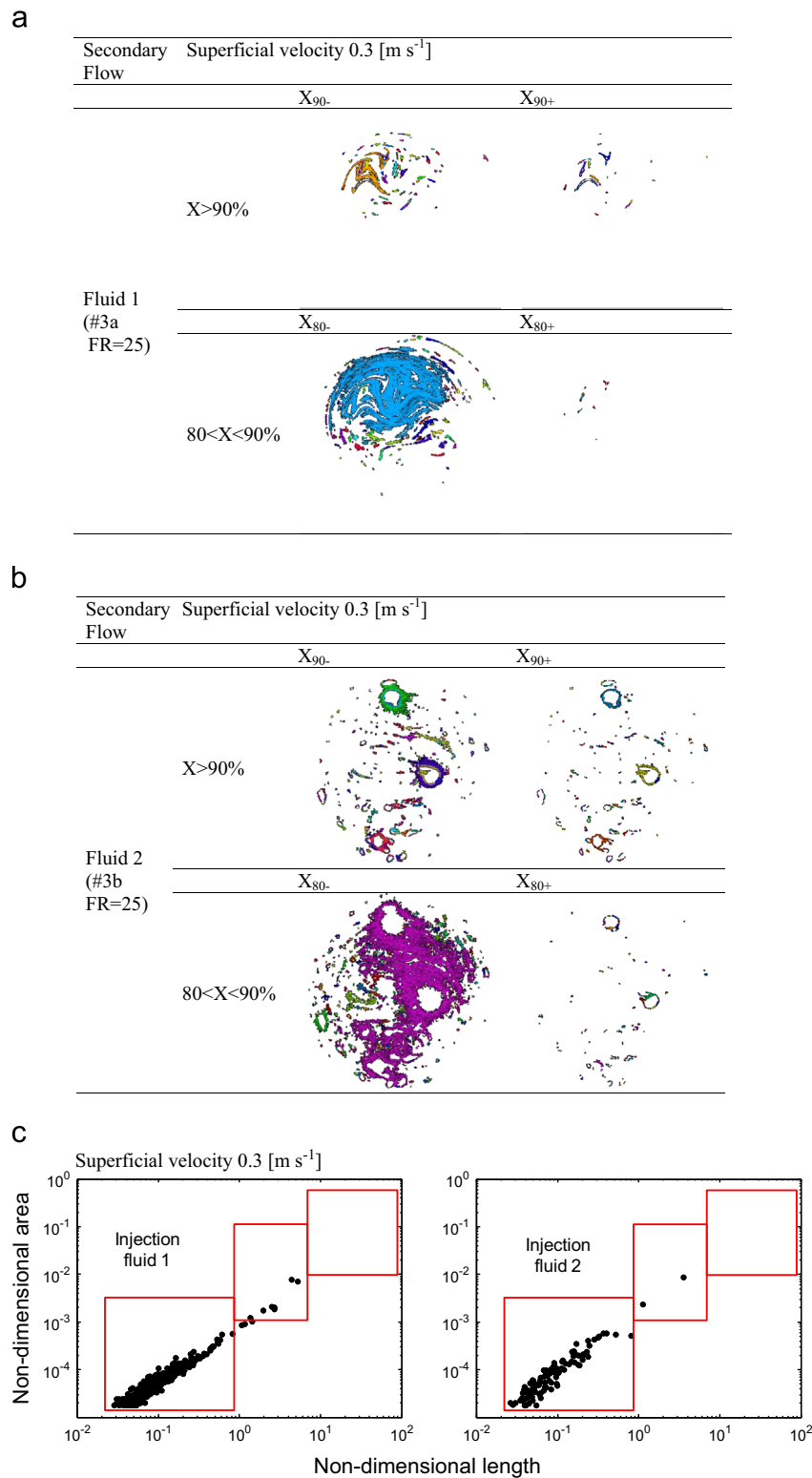
Fig. 12. Illustration of striations detected using the individual striation method for selected ranges of level of mixedness, X, for experiment #3 using the 1″ mixer at $v = 0.3$ m s^{-1} – (a) visualisation of striations with fluid 1 as secondary flow; (b) visualisation of striations with fluid 2 as secondary flow and (c) zonal representation.

wall injection (#4a and #4b) is so poor that only a few spots have a mixing intensity of $X > 90\%$. Fig. 13b shows that all striations are concentrated in zone 1, again indicative of poor mixing.

This work shows that each of the presented methods is able to detect, to a greater or lesser extent, the effect of changing process parameters. What is important when assessing the appropriateness of these methods to characterise mixing behaviour are the

requirements of the downstream process, or alternatively the required product attribute. If the size or distribution of sizes of any unmixed component is critical, then the maximum striation area and areal distribution methods would be appropriate, since in tandem these enable both the size and concentration of any unmixed 'lumps' to be obtained. They can also be used more intelligently, since the areal distribution method enables
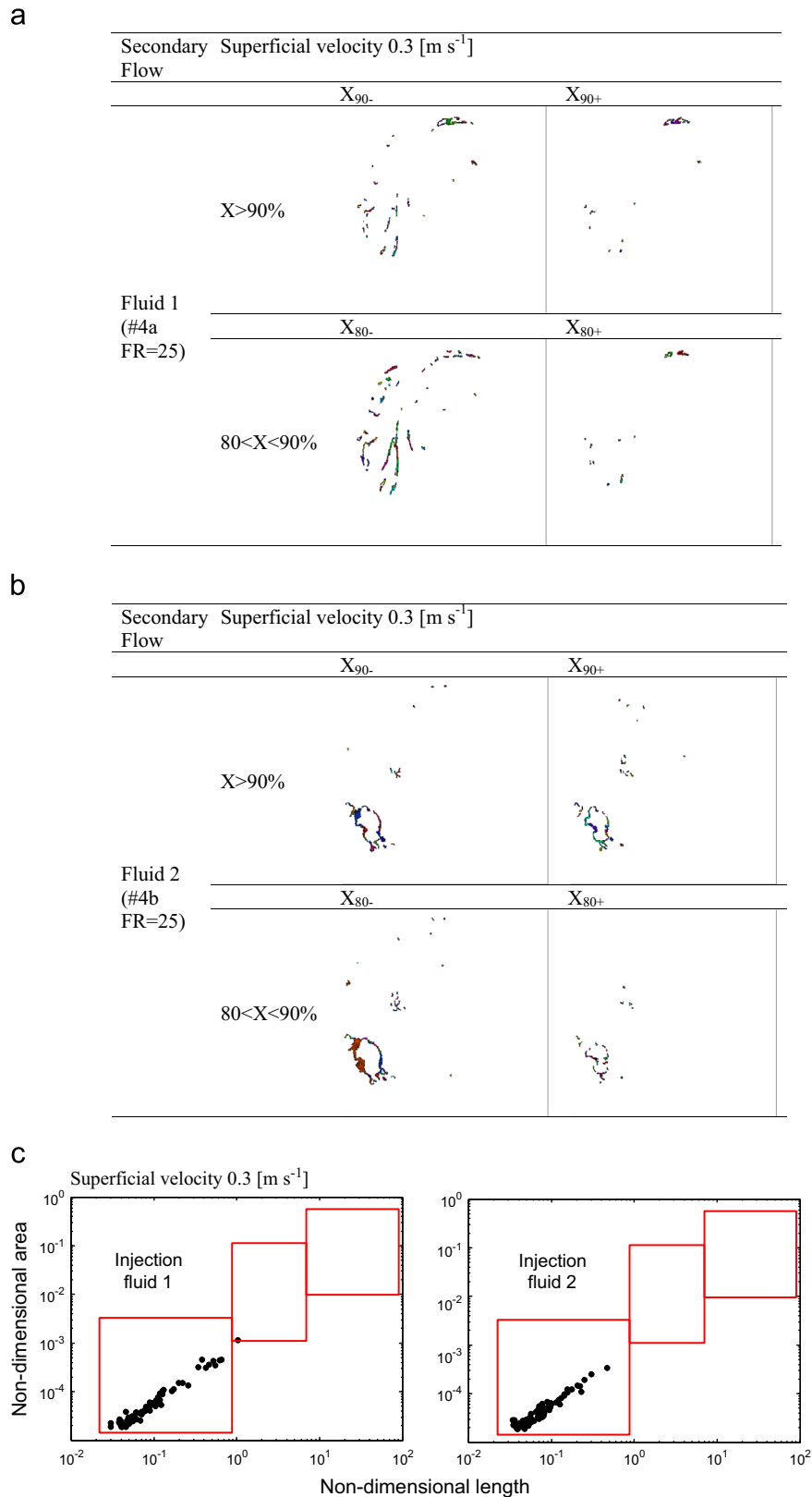
Fig. 13. Illustration of striations detected using the individual striation method for selected ranges of level of mixedness, X, for experiment #4 using the 1″ mixer at $v = 0.3$ m s^{-1} – (a) visualisation of striations with fluid 1 as secondary flow; (b) visualisation of striations with fluid 2 as secondary flow and (c) zonal representation.

interrogation of striations within the mixture as a function of concentration, this might be important for reactive systems where concentration ranges may need to be controlled to prevent formation of unwanted side products. Whilst CoV enables the range of concentration to be considered in a global sense, it does not consider the local distribution of the concentration, which gives the areal distribution method and individual striation methods a clear advantage.

5. Conclusions

Analysis of PLIF images has been performed to determine the mixing performance of Kenics KM static mixers for the blending of two non-Newtonian shear thinning fluids as a function of velocity, scale, flow ratio, viscosity ratio and injection position of the secondary flow. Analysis of the data using CoV for intensity of segregation and maximum striation area for scale of segregation have that shown in some cases one of the measures gives misleading results if the other is ignored, which is a well-known problem in the literature (e.g. Kukukova et al., 2009). The areal distribution method presented by Alberini et al. (2014) which considers the distribution of the cross-sectional area as a function of the level of mixedness, has been used in combination with a new individual striation method to provide an improved and more detailed measure of the mixing performance.

The areal distribution method has been demonstrated to give a more consistent measure of mixing performance than either CoV or maximum striation thickness if either of these quantities are used in isolation. An added advantage is the ability to assess the performance according to the level of mixedness X, which can be defined based on the requirements of the downstream process. Depending on the choice of range of X subtle differences in the performance between the different scales have been identified. In all cases, use of the more viscous fluid 2 as the secondary flow has a detrimental effect on mixing, due to the slow diffusion and incorporation of the viscous fluid filaments so formed. All of the analysis methods were able to identify that use of wall injection of the secondary flow at the mixer inlet led to a very poor mixing performance and this operating condition is not recommended.

Acknowledgements

References

Adamiak, I., Jaworski, Z., 2001. An experimental investigation of the non-Newtonian liquid flow in a Kenics static mixer. Inzynieria Chem. I Proces. 22, 175–180.

Alberini, F., Simmons, M.J.H., Ingram, A., Stitt, E.H., 2014. Use of an areal distribution of mixing intensity to describe blending of non-newtonian fluids in a kenics KM static mixer using PLIF. AIChE J. 60 (1), 332–342.

Chandra, K.G., Kale, D.D., 1992. Pressure-drop for laminar-flow of viscoelastic fluids in static mixers. Chem. Eng. Sci. 47, 2097–2100.

Etchells III, A.W., Meyer, C.F., 2004. Mixing in pipelines. In: Paul, E.L., Atiemo-Obeng, V.A., Kresta, S.M. (Eds.), Handbook of Industrial Mixing (2004) – Science and Practice. John Wiley & Sons, New Jersey, pp. 391–478.

Kukukova, A., Aubin, J., Kresta, S.M., 2009. A new definition of mixing and segregation: three dimensions of a key process variable. Chem. Eng. Res. Des. 87, 633–647.

Kukukova, A., Aubin, J., Kresta, S., 2011. Measuring the scale of segregation in mixing data. Can. J. Chem. Eng. 89 (5), 1122–1138.

Peryt-Stawiarska, S. Jaworski, 2011. The CFD numerical analysis of non-Newtonian fluid flow through Kenics static mixer. Przem. Chem. 90, 1661–1663.

Peryt-Stawiarska, S., Jaworski, Z., 2008. Fluctuations of the non-Newtonian fluid flow in a Kenics static mixer: an experimental study. Pol. J. Chem. Technol. 10, 35–37.

Rafiee, M., Simmons, M.J.H., Ingram, A., Stitt, E.H., 2013. Development of positron emission particle tracking for studying laminar mixing in Kenics static mixer. Chem. Eng. Res. Des. 91 (11), 2106–2113.

Rahmani, R.K., Keith, T.G., 2006. Numerical simulation and mixing study of pseudoplastic fluids in an industrial helical static mixer. J. Fluids Eng.-Trans. ASME 128 (3), 467–480.

Shah, N.F., Kale, D.D., 1991. Pressure drop for laminar flow of non-Newtonian fluids in static mixers. Chem. Eng. Sci. 46, 2159–2161.

Spencer, R.S., Wiley, R.M., 1951. The mixing of very viscous liquids. J. Colloid Sci. 6 (2), 133–145.

Tozzi, E.J., Mccarthy, K.L., Bacca, L.A., Hartt, W.H., Mccarthy, M.J., 2012. Quantifying mixing using magnetic resonance imaging. J. Vis. Exp.: JoVE, e3493

Ventresca, A.L., Cao, Q., Prasad, A.K., 2002. The influence of viscosity ratio on mixing effectiveness in a two-fluid laminar motionless mixer. Can. J. Chem. Eng. 80, 614–621.